Science Arts & Métiers (SAM)

is an open access repository that collects the work of Arts et Métiers Institute of Technology researchers and makes it freely available over the web where possible.

Quantifying discretization errors for soft tissue simulation in computer assisted surgery: A preliminary study

Michel Duprez [a], Stéphane Pierre Alain Bordas [b], Marek Bucki [c], Huu Phuoc Bui [d], Franz Chouly [e,*], Vanessa Lleras [f], Claudio Lobos [g], Alexei Lozinski [d], Pierre-Yves Rohan [h], Satyendra Tomar [b]

[a] *Laboratoire Jacques-Louis Lions (LJLL) UMR 7598 CNRS, Sorbonne Université, Campus de Jussieu, 4 Place Jussieu, Paris 75005, France*
[b] *Faculté des Sciences, de la Technologie et de la Communication, Department of Computational Engineering Sciences, Université du Luxembourg, Maison du Nombre, 6, Avenue de la Fonte L-4364 Esch-sur-Alzette, Luxembourg*
[c] *Texisense, 2, Avenue des Puits, Montceau-les-Mines 71300, France*
[d] *Laboratoire de Mathématiques de Besançon, UMR CNRS 6623, Université Bourgogne Franche-Comté, 16, route de Gray, Besançon Cedex 25030, France*
[e] *Institut de Mathématiques de Bourgogne, UMR CNRS 5584, Université Bourgogne Franche-Comté, Faculté des Sciences Mirande, 9 avenue Alain Savary BP 47870, Dijon Cedex 21078, France*
[f] *Institut de Mathématiques et de Modélisation de Montpellier, Université Montpellier, Case courrier 051, Place Eugène Bataillon, Montpellier Cedex 34095, France*
[g] *Departamento de Informática, Universidad Técnica Federico Santa María, Av. Vicuña Mackenna 3939, San Joaquín, Santiago 8940897, Chile*
[h] *LBM/Institut de Biomécanique Humaine Georges Charpak, Arts et Metiers ParisTech, 151 Boulevard de l'Hôpital, Paris 75013, France*

A B S T R A C T

Errors in biomechanics simulations arise from modelling and discretization. Modelling errors are due to the choice of the mathematical model whilst discretization errors measure the impact of the choice of the numerical method on the accuracy of the approximated solution to this specific mathematical model. A major source of discretization errors is mesh generation from medical images, that remains one of the major bottlenecks in the development of reliable, accurate, automatic and efficient personalized, clinically-relevant Finite Element (FE) models in biomechanics. The impact of mesh quality and density on the accuracy of the FE solution can be quantified with *a posteriori* error estimates. Yet, to our knowledge, the relevance of such error estimates for practical biomechanics problems has seldom been addressed, see Bui et al. (2018). In this contribution, we propose an implementation of some *a posteriori* error estimates to quantify the *discretization errors* and to optimize the mesh. More precisely, we focus on error estimation for a user-defined quantity of interest with the Dual Weighted Residual (DWR) technique. We test its applicability and relevance in three situations, corresponding to experiments in silicone samples and computations for a tongue and an artery, using a simplified setting, i.e., plane linearized elasticity with contractility of the soft tissue modeled as a pre-stress. Our results demonstrate the feasibility of such methodology to estimate the actual solution errors and to reduce them economically through mesh refinement.

* Corresponding author.
E-mail addresses: mduprez@math.cnrs.fr (M. Duprez), stephane.bordas@northwestern.edu (S.P.A. Bordas), marek.bucki@texisense.com (M. Bucki), huu-phuoc.bui@math.cnrs.fr (H.P. Bui), franz.chouly@u-bourgogne.fr (F. Chouly), vanessa.lleras@umontpellier.fr (V. Lleras), clobos@inf.utfsm.cl (C. Lobos), alexei.lozinski@univ-fcomte.fr (A. Lozinski), pierre-yves.rohan@ensam.eu (P.-Y. Rohan), tomar.sk@iitkalumni.org (S. Tomar).

1. Introduction

Patient-specific finite element models of soft tissue and organs receive a large amount of interest. Such finite element models are widely employed to investigate both the underlying mechanisms that drive normal physiology of biological soft tissues and the mechanical factors that contribute to the onset and development of diseases such as tumour growth [1], atherosclerosis or aneurysms [2], or multilevel lumbar disc degenerative diseases [3], to name a few. Finite element models are also valuable tools that contribute to the development of medical devices such as, for example, vascular stent-grafts [4], and have the potential to improve prevention strategies [5], surgical planning [6] and pedagogical simulators for medical training [7].

In this context, one major issue is meshing, since the reliability of the predicted mechanical response arising from computer simulation heavily relies on the quality of the underlying finite element mesh: if some elements of the mesh are too distorted or if the mesh is too coarse in some regions, the numerical solution may deteriorate significantly [8].

The patient-specific mesh has to be built from segmented medical images (CT, MRI, ultra-sound), and has to conform to anatomical details with potentially complex topologies and geometries [9], which led to the design of algorithms that aim to optimize the quality of the generated mesh by reducing the distortion of the elements [10]. These algorithms may also have to satisfy a number of additional constraints such as minimizing human intervention (automation), preservation of certain important anatomical details or robustness with respect to data [11]. In general the quality of a given mesh is assessed through purely geometrical criteria, that allow in some way to quantify the distortion of the geometry of the elements and how far they are from their ideal shape [12].

Beyond mesh quality, mesh density is another, related, parameter which must be controlled during biomechanics simulations. Solutions must be obtained on commodity hardware within clinical time scales: milliseconds (for surgical training); minutes (for surgical assistance); hours (for surgical planning). Therefore, and although this would lead to the most accurate solution, it is impractical to use a uniformly fine mesh over the whole domain. This remark begs the question: "given a tolerable error level, what is the coarsest possible mesh which will provide the required accuracy." This leads to the notion of "mesh optimality," which is achieved for an optimal balance between the accuracy in a given quantity of interest to the user and the associated computational cost. It is probably intuitively understood that this "optimality" criterion, and the resulting optimized mesh both depend on the quantity of interest and that, in general, the optimal mesh will be non-uniform, displaying local refinement around specific regions. A possible criterion for mesh adaptation can be any *a priori* knowledge of the problem or its solution such as geometry, material properties or boundary layers *e.g.,* localized loads, contacts, sharp features, material interfaces. Similarly, knowledge of the quantity of interest can help guide local mesh refinement. Nevertheless, such mesh refinement guidelines are generally *ad hoc* and cannot guarantee the resulting mesh will be optimal.

To summarize, the choice of an optimal mesh, in particular its local refinement level for given problems and quantities of interest remains an open issue. Moreover, without knowing the finite element solution itself, it is practically impossible to quantify the adequacy of a given mesh only from heuristics or other *ad hoc* criteria derived from a priori knowledge of the problem or its exact solution.

As a result, we aim at addressing the following two questions in this paper:

1. For a patient-specific finite element computation, how can we provide some information to the user about the accuracy of the numerical solution, namely how can we compute an approximate *discretization error* caused by the choice of the mesh ? By *discretization error*, we mean the difference between the finite element solution and the exact solution of the same boundary value problem on the same geometry.
2. How can the numerical solution be used to optimize the mesh in the critical regions only, to achieve maximum accuracy for a given computational cost, or, conversely, to achieve a given accuracy with a minimum computational cost?

For the sake of simplicity we do not consider

1. *modelling errors*, which arise due to the approximation of the geometry, physical assumptions, and uncertainty on material parameters,
2. *numerical errors*, which arise due to linearization, iterative solvers, and machine precision.

In this paper, we investigate the capability of *a posteriori* error estimates [13,14] to provide useful information about the *discretization error*. *A posteriori* error estimates are quantities computed from the numerical solution, that indicate the magnitude of the local error. These estimates are at the core of mesh adaptive techniques [15]. Many *a posteriori* error estimation methods have been developed in the numerical analysis community. These methods have different theoretical and practical properties. However, despite their great potential, error estimates, to the best of our knowledge, have rarely

been considered for patient-specific finite element simulations in the biomechanical community. The only reference known to us which addresses discretization error estimation in biomechanics is the very recent paper [16] who consider simple but real-time error estimation approaches for needle insertion.

We limit our study to a simplified setting in order to gain preliminary insights into the behaviour of such *a posteriori* error estimates and to address the first technical difficulties. We focus on two-dimensional linear elasticity (plane strain) problems, with simple boundary conditions (prescribed displacements and tractions), and we assume triangular meshes. This is somehow restrictive in comparison to current practice in soft tissue simulation. Among the existing *a posteriori* error estimates, we focus on Dual Weighted Residuals (DWR), as presented in, *e.g.*, [17,18]. Indeed this method allows to estimate the error for a given quantity of interest. As a matter of fact, for the majority of applications, controlling the error in the energy norm is not relevant, and the error must be controlled for a *specific* quantity of interest to the user (*e.g.*, shear stress or strain intensity at specific locations). The DWR method is conveniently implemented in the standard finite element library FEniCS [19] and we make use of the implementation described in detail in the paper of Rognes and Logg [20], with some modifications. Our adaptive algorithm has been made freely available and can be downloaded from the Figshare repository.[1]

This paper is organized as follows. In Section 2, we present the linear elastic problem, the corresponding finite element method, the *a posteriori* error estimates as well as the algorithm for mesh refinement. In Section 3, we consider three test-cases, a first one for experimental validation, and two others inspired by patient-specific biomechanics, where the current methodology is applied. The results are discussed in Section 4. A conclusion follows in Section 5.

2. Material and methods

We first present the general problem considered in this contribution, that represents a simplified setting for contractile soft tissue simulation. We then describe in detail the computation of the *a posteriori* error estimate: a global estimator that provides an estimation of the *discretization error* and a local estimator that drives the mesh refinement. We end this section with the description of a simple algorithm for mesh refinement.

We first introduce some useful notations. In what follows, bold letters such as $\mathbf{u}$, $\mathbf{v}$, indicate vector or tensor valued quantities, while the capital ones (*e.g.*, $\mathbf{V}$, $\mathbf{K}$) represent functional sets involving vector fields. As usual, we denote by $L^2(\cdot)$ the space of square-integrable functions, and $(H^s(\cdot))^d$, $s \in \mathbb{R}$, $d = 1, 2, 3$, the Sobolev spaces in one, two or three space dimensions. In the sequel the symbol $|\cdot|$ will either denote the Euclidean norm in $\mathbb{R}^d$, or the measure of a domain in $\mathbb{R}^d$.

2.1. Setting: a "toy" boundary value problem in linear elasticity

We consider an elastic body whose reference configuration is represented by the domain Ω in $\mathbb{R}^2$. We consider the plane strain formulation, and allow only small deformations. We suppose that $\partial \Omega$ consists of two disjoint parts Γ_D and Γ_N, with meas$(\Gamma_D) > 0$. The unit outward normal vector on $\partial \Omega$ is denoted by $\mathbf{n}$. A displacement $\mathbf{u}_D = \mathbf{0}$ is applied on Γ_D, and the body is subjected to volume forces $\mathbf{f} \in (L^2(\Omega))^2$ and surface loads $\mathbf{F} \in (L^2(\Gamma_N))^2$. For two displacement fields $\mathbf{v}$ and $\mathbf{w}$ defined on Ω, we introduce the bilinear form

$$a(\mathbf{v}, \mathbf{w}) := \int_\Omega \boldsymbol{\sigma}(\mathbf{v}) : \boldsymbol{\varepsilon}(\mathbf{w}) \, \mathrm{d}\mathbf{x},$$

which represents the (internal) virtual work associated to passive elastic properties. The notation $\boldsymbol{\varepsilon}(\mathbf{v}) = \frac{1}{2}(\nabla \mathbf{v} + \nabla \mathbf{v}^T)/2$ represents the linearized strain tensor field, and $\boldsymbol{\sigma} = (\sigma_{ij})$, $1 \leq i, j \leq 2$, stands for the stress tensor field, assumed to be given by Hooke's law. The linear form

$$\ell_E(\mathbf{w}) := \int_\Omega \mathbf{f} \cdot \mathbf{w} \, \mathrm{d}\mathbf{x} + \int_{\Gamma_N} \mathbf{F} \cdot \mathbf{w} \, \mathrm{d}s$$

stands for the virtual work of external loads in the body and on its surface. Finally we represent in a very simplified manner the active properties of soft tissue as a linear anisotropic pre-stress

$$\ell_A(\mathbf{w}) := -\beta T \int_{\omega_A} (\boldsymbol{\varepsilon}(\mathbf{w})\mathbf{e}_A) \cdot \mathbf{e}_A \, \mathrm{d}\mathbf{x},$$

where ω_A is the part of the body where muscle fibers are active, $T \geq 0$ is a scalar which stands for the tension of the fibers, $\mathbf{e}_A$ is a field of unitary vectors that stands for muscle fibers orientation, and $\beta \in [0, 1]$ is the activation parameter. When $\beta = 0$ there is no activation of the muscle fibers, and the value $\beta = 1$ corresponds to the maximum activation. This modelling can be viewed as a linearization of some more sophisticated active stress models of contractile tissues (see, *e.g.*, [21,22]).

We want to solve the following weak problem

$$\begin{cases} \text{Find a displacement } \mathbf{u} \in \mathbf{V} \text{ such that} \\ a(\mathbf{u}, \mathbf{v}) = \ell(\mathbf{v}), \quad \forall \mathbf{v} \in \mathbf{V}, \end{cases} \tag{1}$$

where $\ell(\cdot) = \ell_E(\cdot) + \ell_A(\cdot)$, and where $\mathbf{u}$ and $\mathbf{v}$ lie in the space of admissible displacements

$$\mathbf{V} := \left\{ \mathbf{v} \in H^1(\Omega)^2 \mid \mathbf{v} = \mathbf{0} \text{ on } \Gamma_D \right\}.$$

From the displacement field, we are interested in computing a linear quantity

$$J : \mathbf{V} \ni \mathbf{u} \mapsto J(\mathbf{u}) \in \mathbb{R}, \tag{2}$$

which can be defined according to a specific application and the interest of each practitioner. Thereby, the quantity J will be called *quantity of interest (QoI)*. We will provide its expression(s) for each test case (see Section 3).

2.2. Finite element method

Consider a family of meshes $(\mathcal{K}_h)_{h>0}$ constituted of triangles and assumed to be subordinate to the decomposition of the boundary $\partial\Omega$ into Γ_D and Γ_N. For a mesh $\mathcal{K}_h$, we denote by $\mathcal{E}_h$ the set of edges, by $\mathcal{E}_h^{int} := \{E \in \mathcal{E}_h : E \subset \Omega\}$ the set of interior edges, and by $\mathcal{E}_h^N := \{E \in \mathcal{E}_h : E \subset \Gamma_N\}$ the set of boundary edges that correspond to Neumann conditions (we assume that any boundary edge is either inside Γ_N or inside Γ_D). For an element K of $\mathcal{K}_h$, we set $\mathcal{E}_K$ the set of edges of K, $\mathcal{E}_K^{int} := \mathcal{E}_K \cap \mathcal{E}_h^{int}$ and $\mathcal{E}_K^N := \mathcal{E}_K \cap \mathcal{E}_h^N$. We also assume that each element K is either completely inside ω_A or completely outside it. Let $\boldsymbol{\sigma}$ be a second-order tensorial field in Ω, which is assumed to be piecewise continuous. We define the jump of $\boldsymbol{\sigma}$ across an interior edge E of an element K, at a point $\mathbf{y} \in E$, as follows

$$[\![\boldsymbol{\sigma}]\!]_{E,K}(\mathbf{y}) := \lim_{\alpha \to 0^+} (\boldsymbol{\sigma}(\mathbf{y} + \alpha\mathbf{n}_{E,K}) - \boldsymbol{\sigma}(\mathbf{y} - \alpha\mathbf{n}_{E,K}))\mathbf{n}_{E,K},$$

where $\mathbf{n}_{E,K}$ is the unit normal vector to E, pointing out of K.

The finite element space $\mathbf{V}_h \subset \mathbf{V}$ is built upon continuous Lagrange finite elements of degree $k = 1, 2$ (see, *e.g.*, [23]), *i.e.*

$$\mathbf{V}_h := \left\{ \mathbf{v}_h \in (\mathcal{C}^0(\overline{\Omega}))^d : \mathbf{v}_{h|K} \in (\mathbb{P}_k(K))^d, \forall K \in \mathcal{K}_h, \mathbf{v}_h = \mathbf{0} \text{ on } \Gamma_D \right\}.$$

Problem (1) is approximated by

$$\begin{cases} \text{Find } \mathbf{u}_h \in \mathbf{V}_h \text{ such that} \\ a(\mathbf{u}_h, \mathbf{v}_h) = \ell(\mathbf{v}_h), \qquad \forall \mathbf{v}_h \in \mathbf{V}_h. \end{cases} \tag{3}$$

2.3. Goal-oriented error estimates

We compute goal-oriented error estimates using the Dual Weighted Residual (DWR) technique [17,18]. We follow the framework described in [20], with some minor changes and adaptations.

Let us consider $\mathbf{u}_h$ the solution to Problem (3). The weak residual is defined for all $\mathbf{v} \in \mathbf{V}$ by

$$r(\mathbf{v}) := \ell(\mathbf{v}) - a(\mathbf{u}_h, \mathbf{v}).$$

Let $\mathbf{z}$ denote the solution to the dual problem:

$$\begin{cases} \text{Find } \mathbf{z} \in \mathbf{V} \text{ such that} \\ a(\mathbf{v}, \mathbf{z}) = J(\mathbf{v}), \qquad \forall \mathbf{v} \in \mathbf{V}. \end{cases} \tag{4}$$

The DWR method, in a linear setting, relies on the fundamental observation that

$$J(\mathbf{u}) - J(\mathbf{u}_h) = a(\mathbf{u}, \mathbf{z}) - a(\mathbf{u}_h, \mathbf{z}) = \ell(\mathbf{z}) - a(\mathbf{u}_h, \mathbf{z}) = r(\mathbf{z}). \tag{5}$$

From this, we design an error estimator of $J(\mathbf{u}) - J(\mathbf{u}_h)$ as an approximation of the residual $r(\mathbf{z})$. We detail the different steps below.

2.3.1. Numerical approximation of the dual problem and global estimator

The exact solution $\mathbf{z}$ to the dual system (4) is unknown in most practical situations, and thus needs to be approximated. Let us consider a finite element space $\widehat{\mathbf{V}}_h \subset \mathbf{V}$. This space is assumed to be finer than $\mathbf{V}_h$, for instance, made of continuous piecewise polynomials of order $k+1$. The approximation $\widehat{\mathbf{z}}_h$ of the solution to the dual problem $\mathbf{z}$ is obtained by solving the following approximate dual problem

$$\begin{cases} \text{Find } \widehat{\mathbf{z}}_h \in \widehat{\mathbf{V}}_h \text{ such that} \\ a(\widehat{\mathbf{v}}_h, \widehat{\mathbf{z}}_h) = J(\widehat{\mathbf{v}}_h), \qquad \forall \widehat{\mathbf{v}}_h \in \widehat{\mathbf{V}}_h. \end{cases} \tag{6}$$

We define

$$\eta_h := |r(\widehat{\mathbf{z}}_h)| \tag{7}$$

as the *global estimator* that approximates the residual $|r(\mathbf{z})|$.

2.3.2. Derivation of local estimators

Following [18,20], we provide a *local estimator* of the error $|J(\mathbf{u}) - J(\mathbf{u}_h)|$, that can be written in a general form

$$\sum_{K \in \mathcal{K}_h} \eta_K, \quad \eta_K := \left| \int_K R_K \cdot (\widehat{\mathbf{z}}_h - i_h \widehat{\mathbf{z}}_h) \mathrm{d}\mathbf{x} + \sum_{E \in \mathcal{E}_K} \int_E R_{E,K} \cdot (\widehat{\mathbf{z}}_h^i - i_h \widehat{\mathbf{z}}_h) \mathrm{d}s \right|, \quad \forall K \in \mathcal{K}_h, \tag{8}$$

where the notation i_h stands for the Lagrange interpolant onto $\mathbf{V}_h$.

The local element-wise and edge-wise residuals are given explicitly by

$$R_K := \mathbf{f}_K + \mathbf{div}\, \boldsymbol{\sigma}_A(\mathbf{u}_h)$$

and

$$R_{E,K} := \begin{cases} -\dfrac{1}{2} [\![\boldsymbol{\sigma}_A(\mathbf{u}_h)]\!]_{E,K} & \text{if } E \in \mathcal{E}_K^{int}, \\ \mathbf{F}_E - \boldsymbol{\sigma}_A(\mathbf{u}_h) \mathbf{n}_{E,K} & \text{if } E \in \mathcal{E}_K^N, \end{cases}$$

where

$$\boldsymbol{\sigma}_A(\mathbf{u}^h) := \boldsymbol{\sigma}(\mathbf{u}^h) + \beta T (\mathbf{e}_A \otimes \mathbf{e}_A) \chi_A.$$

The notation χ_A stands for the indicator function of ω_A, *i.e.* $\chi_A = 1$ in ω_A and $\chi_A = 0$ elsewhere. The quantity $\boldsymbol{\sigma}_A(\mathbf{u}^h)$ represents the sum of passive and active contributions within the stress field. The quantity $\mathbf{f}_K$ (resp. $\mathbf{F}_E$) is a computable approximation of $\mathbf{f}$ (resp. $\mathbf{F}$).

The following bound always holds

$$\eta_h \leq \sum_{K \in \mathcal{K}_h} \eta_K,$$

since compensation effects (balance between positive and negative local contributions) can occur for η_h, see, *e.g.*, [24]. Thus η_h is expected to be sharper than $\sum_{K \in \mathcal{K}_h} \eta_K$. In practice, $\sum_{K \in \mathcal{K}_h} \eta_K$ aims at quantifying the local errors for mesh refinement.

Remark 2.1. Each local estimator η_K is made up of two contributions. On one hand, the residuals R_K and $R_{E,K}$ represent the local error in the natural norm. On the other hand, the contribution $(\widehat{\mathbf{z}}_h^i - i_h \widehat{\mathbf{z}}_h)$ coming from the dual problem can be interpreted as a *weight* (or a sensitivity factor) that measures the local impact on the quantity of interest $J(\cdot)$, see, *e.g.*, [18, Remark 3.1].

Remark 2.2. In [20] the local residuals R_K and $R_{E,K}$ are computed implicitly through local problems, in a generic fashion. No significant difference has been observed numerically between the technique of [20] and an explicit computation.

Remark 2.3. We have chosen to compute $\widehat{\mathbf{z}}_h$ through the approximate dual system computed in $\widehat{\mathbf{V}}_h \subset \mathbf{V}$ (the space made of continuous piecewise polynomials of order $k+1$, *i.e.* one order higher than $\mathbf{V}_h$). Other strategies are possible: see, *e.g.*, [18, Section 5.1] for a discussion. For example, the authors of [20] use extrapolation of the approximate dual system computed in $\mathbf{V}_h$. We can also mention [25], where the weight is estimated using a residual *a posteriori* error estimate for the dual system, approximated in $\mathbf{V}_h$. The aforementioned techniques are cheaper since the same space is used for the primal and dual solutions, but they can be less accurate.

2.4. Algorithm for goal-oriented mesh refinement

In the last sections, we have described the different steps to construct the global and local error estimators. Using the Dörfler marking strategy [26], we now describe, in Algorithm 1, a simple algorithm to refine the mesh by taking into account these quantities. In this algorithm, there are two independent numerical parameters: first a parameter $0 < \alpha \leq 1$ that controls the level of refinement in Dörfler marking, and then a tolerance threshold $\varepsilon > 0$ for the global estimator, that serves as a stopping criterion.

The FEniCS script, as well as a mesh (the tongue mesh described in Section 3.2), are freely available online, and can be downloaded from the Figshare repository.[2]

3. Results

We present numerical results for three different test cases. First we validate our methodology by confrontation with experimental measurements made on silicone samples (Section 3.1). Then we present the biomechanical response of both a human tongue (Section 3.2) and an arterial wall (Section 3.3) simulated using finite element analysis. This two latter

---

[2] https://figshare.com/articles/Quantifying_discretization_errors_for_softtissue_simulation_in_computer_assisted_surgery_a_preliminary_study/8128178

examples are inspired from studies [9,27], respectively. We propose to assess the discretization error for the two quantities of interest

$$J_1(\mathbf{u}) := \int_\omega (u_x + u_y)\, d\mathbf{x} \quad \text{and} \quad J_2(\mathbf{u}) := \int_\omega \text{div } \mathbf{u}\, d\mathbf{x}, \qquad (9)$$

where u_x and u_y are the two components of $\mathbf{u}$ in a Cartesian basis. The first quantity $J_1(\mathbf{u})$ is physically related to the displacement in the region of interest $\omega \subset \Omega$. This corresponds to a quantity that can easily be measured experimentally and that is therefore of practical interest. The second quantity $J_2(\mathbf{u})$ physically corresponds to the internal strain $I_1 = \text{tr}(\boldsymbol{\varepsilon}(\mathbf{u}))$. This is also of practical interest because many of the mechanisms driving the onset of pathologies are related to shear strains or principal strains. The region of interest ω will be specified in each situation. All the simulations of this section are performed with Lagrange finite elements of degree $k = 2$, and the space $\widehat{\mathbf{V}}_h$ in which $\widehat{\mathbf{z}}_h$ is computed is built from Lagrange finite elements of degree $k = 3$ (except in Section 3.1 where finite elements of degree $k = 1$ are also considered). In Algorithm 1, the parameter α for Dörfler marking is fixed at 0.8, and the stopping criterion ε will be specified for each application. In the following, the exact value of $J(\mathbf{u})$ is unknown but is estimated using computations on a very fine uniform mesh.

Algorithm 1: Refinement algorithm.

Initialization :

　　Select an initial triangulation $\mathcal{K}_h$ of the domain Ω.

　　Build the finite elements spaces $\mathbf{V}_h$ and $\widehat{\mathbf{V}}_h$.

While $\eta_h > \epsilon$ do

　　1. Compute $\mathbf{u}_h \in \mathbf{V}_h$: $a(\mathbf{u}_h, \mathbf{v}_h) = \ell(\mathbf{v}_h), \quad \forall \mathbf{v}_h \in \mathbf{V}_h$.
　　2. Compute $\widehat{\mathbf{z}}_h \in \widehat{\mathbf{V}}_h$: $a(\widehat{\mathbf{v}}_h, \widehat{\mathbf{z}}_h) = J(\widehat{\mathbf{v}}_h), \quad \forall \widehat{\mathbf{v}}_h \in \widehat{\mathbf{V}}_h$.
　　3. Evaluate the global error estimator $\eta_h = |r(\widehat{\mathbf{z}}_h)|$.
　　4. If $\eta_h \leq \varepsilon$, then stop.
　　5. Evaluate the local estimators

$$\eta_K := \left| \int_K R_K \cdot (\widehat{\mathbf{z}}_h - i_h \widehat{\mathbf{z}}_h)\, d\mathbf{x} + \sum_{E \in \mathcal{E}_K} \int_E R_{E,K} \cdot (\widehat{\mathbf{z}}_h^i - i_h \widehat{\mathbf{z}}_h)\, ds \right|, \quad \forall K \in \mathcal{K}_h.$$

　　6. Sort the cells $\{K_1, \ldots, K_N\}$ by decreasing order of η_K.
　　7. Dörfler marking: mark the first M^* cells for refinement where

$$M^* := \min \left\{ M \in \mathbb{N} \,\middle|\, \sum_{i=1}^M \eta_{K_i} \geq \alpha \sum_{K \in \mathcal{K}_h} \eta_K \right\}.$$

　　8. Refine all cells marked for refinement (and propagate refinement to avoid hanging nodes).
　　9. Update correspondingly the finite element spaces $\mathbf{V}_h$ and $\widehat{\mathbf{V}}_h$.

3.1. Validation using experimental data

Before considering patient-specific geometries, a validation of the effectiveness of the proposed methodology in quantifying the discretization error is carried out in this section. For this purpose, we compare the numerical results with data from the experimental characterization of the tensile behaviour of an unfilled silicone, reported in [28] (see Fig. 1 (left)).

The experimental procedure is briefly recalled here for the sake of clarity. For more informations, the reader is referred to [28]. Simple tensile tests were performed on dumbbell shaped samples of silicone rubber (RTV 141) having an initial gauge length l_0 of 60 mm, a gauge width b_0 of 12 mm and a gauge thickness e_0 of 2 mm. Tested samples were deformed using a universal mechanical testing machine (MTS 4M). Axial force f_A and axial elongation l/l_0 obtained from DIC results were extracted and plotted (reference experimental curve in Fig. 2 below).

A 2-dimensional model of the dumbbell silicone sample in plane stress is constructed. Under small deformations, rubbers exhibit a linear elastic isotropic constitutive relationship. The Poisson's ratio ν is set to 0.45 and the equivalent Young's modulus E is extracted from the Mooney hyperelastic constitutive parameter C_{10} fitted using experimental data and reported in [28] ($E = 4(1 + \nu)C_{10} \simeq 0.812$ MPa). Dirichlet boundary conditions are imposed on the bottom edge of the dumbell silicone sample. The following Neumann boundary condition is imposed on the top edge: $\mathbf{F} = (f_A/(b_0 \times e_0))\mathbf{n}$ such that
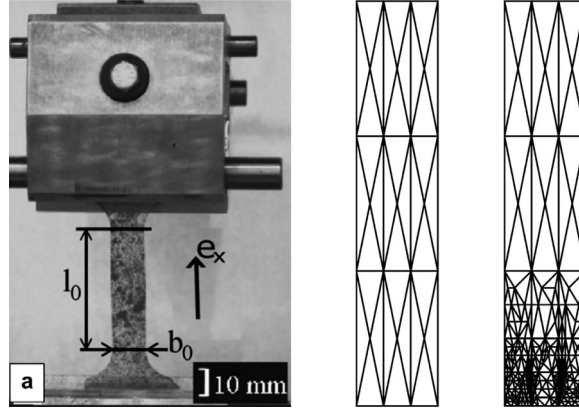
Fig. 1. Tensile test on silicone rubber, from [28] (left). Initial mesh (center) and refined mesh after 5 iterations of Algorithm 1 (right) ($\mathbb{P}_1$ Lagrange FE method).
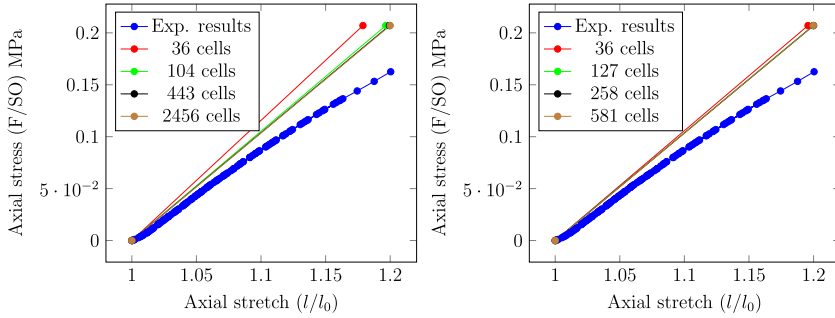

Fig. 2. Unfilled silicone: comparison of the experimental results obtained in [28] with the adaptive FE simulation (Algorithm 1): $\mathbb{P}_1$ (left) and $\mathbb{P}_2$ (right) Lagrange FE method.

Table 1
Predicted stress-stretch slope and relative error with the experimental slope. $\mathbb{P}_1$ Lagrange FE method.

Iteration	Number of cells	Slope	Error
1st iteration	36	1.157	21.83 %
3nd iteration	104	1.053	10.88 %
5th iteration	443	1.038	9.31 %
7th iteration	2456	1.035	9.02 %

Table 2
Predicted stress-stretch slope and relative error with the experimental slope. $\mathbb{P}_2$ Lagrange FE method.

Iteration	Number of cells	Slope	Error
1st iteration	36	1.058	11.42 %
3nd iteration	127	1.037	9.18 %
5th iteration	258	1.035	9.00 %
7th iteration	581	1.035	8.97 %

$\int_{\Gamma_N} \mathbf{F} \cdot \mathbf{n} \, ds = 20$ N. On the other boundaries, we impose a homogeneous Neumann boundary condition ($\mathbf{F} = \mathbf{0}$). We choose the quantity of interest J_1, with $\omega = (3, 9) \times (20, 40)$ mm.

The resulting stress-stretch curves predicted by the numerical method at each adaptive refinement iteration is given in Fig. 2 for $\mathbb{P}_1$ finite elements (left) and $\mathbb{P}_2$ finite elements (right). In the small deformation range (0 to 5% strain), the numerical response is very close to the experimental tensile response. In Fig. 1, we give the initial mesh (center) and the refined mesh after 5 iterations of Algorithm 1 (right).

Quantitative assessment is performed by comparing the slopes of the numerical and experimental tensile responses in the range 1 to 5 %. The slopes and relative percentage error are given in Tables 1 and 2. The errors range from 8 %–20 %. The deviation between the response predicted by the most refined mesh and the experiment can be explained by
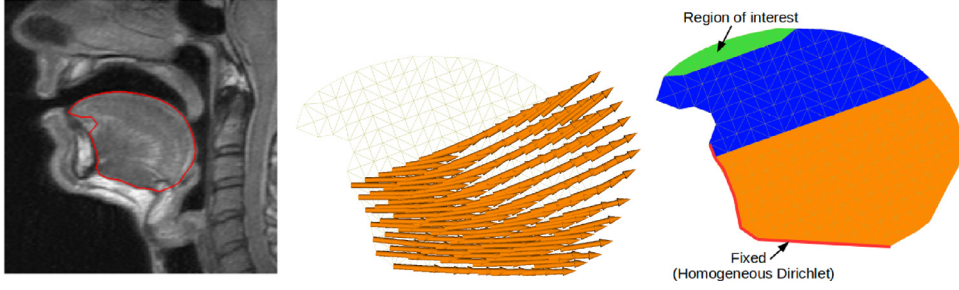
Fig. 3. Tongue model. Initial geometry, from Bijar et al. [9] (left), fiber orientation (center) and region of interest (right). (For interpretation of the references to color in this figure, the reader is referred to the web version of this article.)
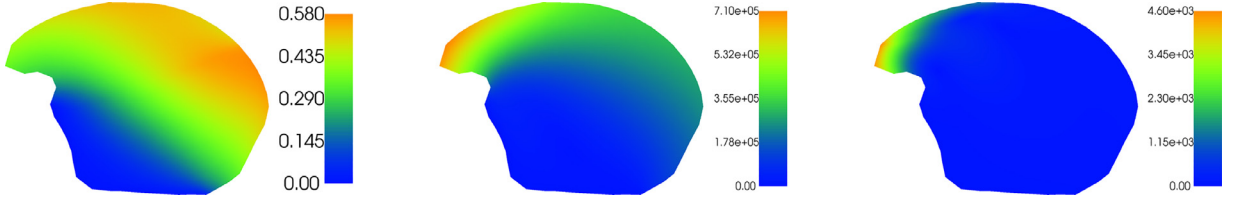

Fig. 4. Tongue model. Displacement (left), dual solutions for J_1 (center) and for J_2 (right).

(i) the error made in [28] in fitting the hyperelastic energy parameters from experimental data (ii) the linearisation procedure performed in this section to extract the equivalent Young's modulus and (iii) the quasi-incompressibility assumption (while in [28] the silicone is assumed to be fully incompressible).

3.2. Human tongue with fiber activation

In this example, we focus on the case study for the activation of the posterior genio-glossus (GGp), that is a lingual muscle located at the root of the tongue and inserted in the front to the mandible. The activation of this muscle compresses the tongue in the lower part and generates a forward and upward movement of the tongue body, because of the incompressibility of tongue tissues, for example during the production of the phonemes /i/ or /s/. The 2D mesh used in this example has been derived from the generic 3D mesh presented in [9] where the authors developed a process to generate subject-specific meshes. More precisely an automatic atlas-based method was proposed that generates subject-specific meshes *via* a registration guided by Magnetic Resonance Imaging. The domain Ω is depicted in Fig. 3 (left). The width and height of the tongue are respectively equal to 73.8 mm and 53.7 mm. For the passive tissue material properties, we use the values reported in [29] based on indentation experiments on a cadavers tongue. The authors initially proposed an incompressible two parameter Yeoh hyperelastic material model and fitted the material constants to the data. In this work, a linear elastic material model is assumed. According to [30], linearisation of the model proposed in [29] yields $E \simeq 0.6$ MPa. For the sake of simplicity Poisson ratio is assumed to be $\nu = 0.4$. No volumic force field is applied: $\mathbf{f} = \mathbf{0}$. The direction of the fibers $\mathbf{e}_A$ is depicted in Fig. 3 (center) and corresponds approximately to the posterior genioglossus muscle [9]. Other parameters for fiber activation have been chosen as $T = 2.10^{-5}$ MPa and $\beta = 1$. The tongue is attached to the hyoid bone and to the mandible, which are supposed to be fixed. This leads to a homogeneous Dirichlet boundary condition such as depicted in Fig. 3 (right). On the remaining part of the boundary a homogeneous Neumann condition ($\mathbf{F} = \mathbf{0}$) is applied. The orange part depicts the region ω_A where fibers are located. The green part depicts the region of interest ω for the computation of J_1 and J_2.

The resulting displacement is depicted in Fig. 4 (left). We computed the relative displacement and the strain intensity, which maximal values are of 5.7 % and 4.8 %, respectively: thus the small displacement and small strain assumptions are both verified in this case. The parameter T has been chosen accordingly in order to respect these assumptions. In Fig. 4, the dual solutions for the quantities of interest J_1 (center) and J_2 (right) are represented. As mentioned in Remark 2.1, the dual solution z is used as a weight in the computation of the estimators, and influences the local refinement.

We present the final mesh after 2 and 8 iterations of Algorithm 1 for both quantities of interest J_1 and J_2, in Fig. 5 and Fig. 6, respectively. We first remark that the refinement occurs in some specific regions such as those near Dirichlet-Neumann transitions and concavities on the boundary. Note as well that the refinement is stronger for J_2 at the boundary of the region of interest ω.

Fig. 7 depicts the relative goal-oriented errors $|J_1(\mathbf{u}) - J_1(\mathbf{u}_h)|/|J_1(\mathbf{u})|$ (left) and $|J_2(\mathbf{u}) - J_2(\mathbf{u}_h)|/|J_2(\mathbf{u})|$ (right) versus N, the number of cells of the mesh, both for uniform refinement (blue) and adaptive refinement (red). The stopping criterion ε has been fixed to 2.10^{-4} and 10^{-6}, respectively. In each situation, we observe that, as expected, adaptive refinement performs better: not only it leads to a lower error but it also converges much faster when the number of cells N is increased.
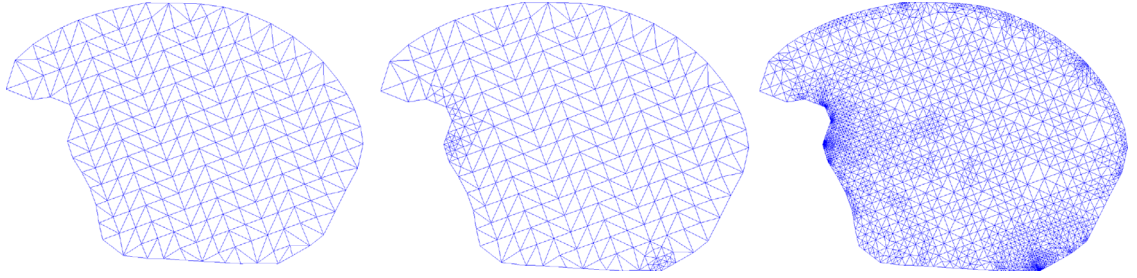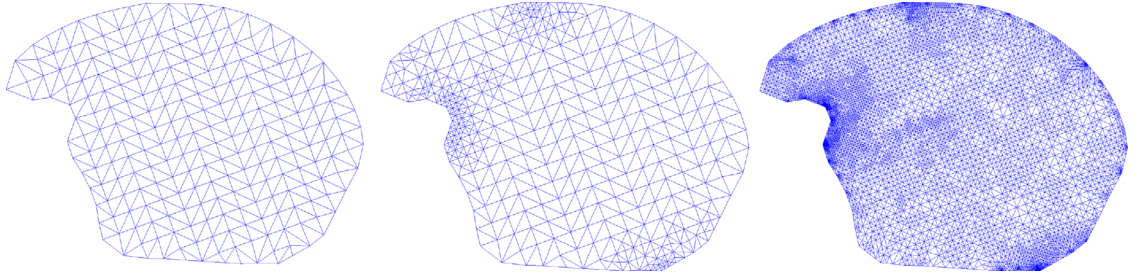
Fig. 5. Tongue mesh. Refinement driven by the QoI J_1. Initial mesh (left) with 426 cells and a relative error of 0.01, adapted meshes after 2 iterations (center) with 523 cells and a relative error of 2.10^{-3} and after 8 iterations (right) with 5143 cells and a relative error of 3.10^{-5}.

Fig. 6. Tongue mesh. Refinement driven by the QoI J_2. Initial mesh (left) with 426 cells and a relative error of 0.03, adapted meshes after 2 iterations (center) with 766 cells and a relative error of 2.10^{-3} and after 8 iterations (right) with 13513 cells and a relative error of 2.10^{-5}.

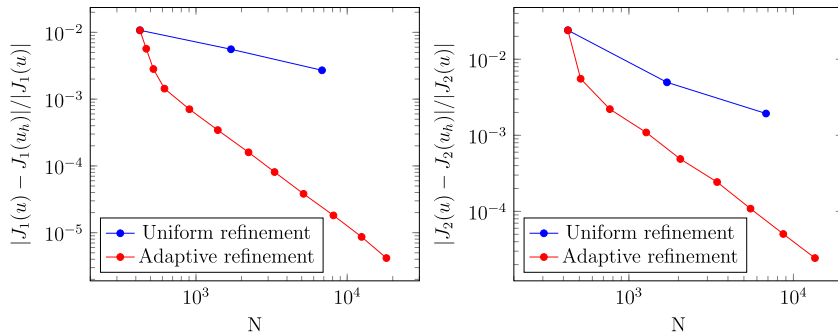**Fig. 7.** Tongue model. Relative error for the QoI J_1 (left) and J_2 (right) *vs.* the number N of cells in the case of uniform (blue) and adaptive (red) refinement. (For interpretation of the references to color in this figure legend, the reader is referred to the web version of this article.)

Finally in Fig. 8 we depict the effectivity indices for the global estimator η_h and the sum of local estimators $\Sigma_K \eta_K$. For both quantities J_1 and J_2, the two estimators provide an estimation of the *discretization error* with an effectivity index around 1. In the case of J_2, we observe a slight overestimation for $\Sigma_K \eta_K$ and a slight underestimation for η_h.

3.3. Human artery with fiber activation

As another example we showcase the performance of the proposed algorithm for the analysis of the mechanical response of an artery with vulnerable coronary plaque to internal loading. Rupture of the cap induces the formation of a thrombus which may obstruct the coronary artery, cause an acute syndrome and the patient death. The geometry (see Fig. 9 (left)) comes from Le Floc'h et al. [27] where the authors develop a methodology to reconstruct the thickness of the necrotic core area and the calcium area as well as the Young's moduli of the calcium, the necrotic core and the fibrosis. Their objective is the prediction of the vulnerable coronary plaque rupture. As represented in Fig. 9 (left), the diameter of the Fibrosis is equal to 5 mm. Following [27], we set different elastic parameters in each region: $E_n = 0.011$ MPa, $\nu = 0.4$ in the necrotic core and $E_s = 0.6$ MPa, $\nu = 0.4$ in the surrounding tissue (contrast $E_s/E_n \simeq 55$). No volumetric force field is applied: $\mathbf{f} = \mathbf{0}$. We consider muscle fibers only in the media layer, where smooth muscle cells are supposed to be perfectly oriented in the circumferential direction $\mathbf{e}_A = \mathbf{e}_\theta$, where $(\mathbf{e}_r, \mathbf{e}_\theta)$ is the basis for polar coordinates, see Fig. 9 (center). Other parameters for fiber activation have been chosen as $T = 0.01$ MPa and $\beta = 1$. As depicted in Fig. 9 (right), the artery is fixed on the red portion of external boundary Γ_D. Elsewhere, on the remaining part of the boundary, a homogeneous Neumann condition is applied: $\mathbf{F} = \mathbf{0}$. In the same figure, the green part represents the region of interest ω, which has been defined in order
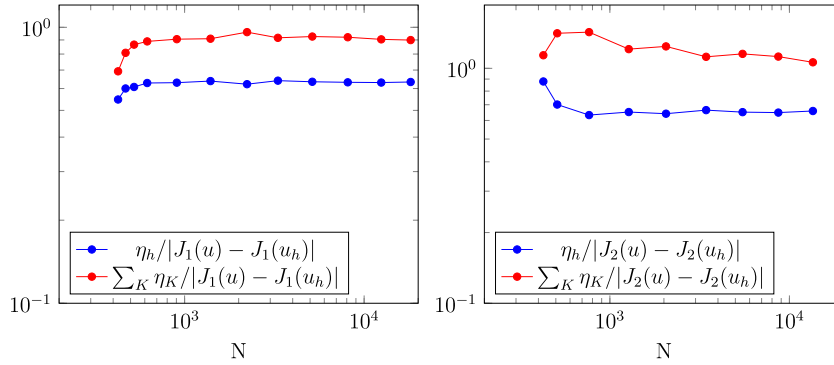
Fig. 8. Tongue model. Effectivity indices for η_h (blue) and $\Sigma_K \eta_K$ vs. the number N of cells for the QoI J_1 (left) and J_2 (right). (For interpretation of the references to color in this figure legend, the reader is referred to the web version of this article.)
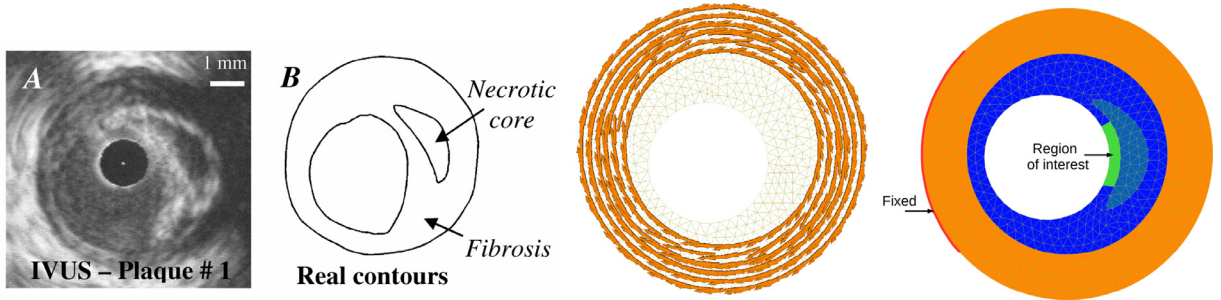

Fig. 9. Artery model. Geometry, from Le Floc'h et al. [27] (left), fiber orientation (center) and region of interest (right).
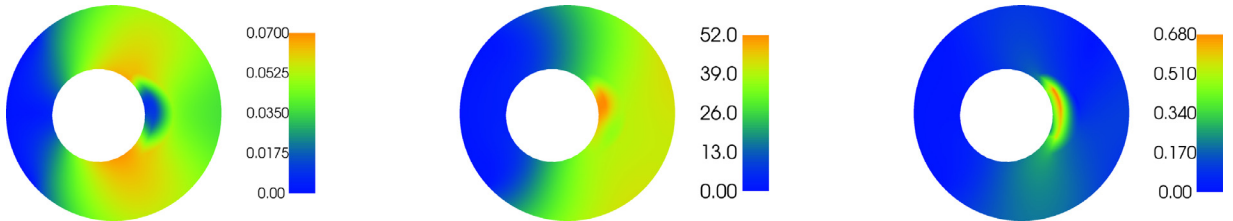

Fig. 10. Artery model. Displacement (left), dual solution for J_1 (center) and for J_2 (right).

to be relevant in the study of vulnerable coronary plaque rupture. As in the previous example, we computed the relative displacement and the strain intensity, and their maximal values are of 6.15 % and 0.3 %, respectively. This ensures that small displacement and small strain assumptions are verified. Fig. 10 depicts the magnitude of the solution in terms of displacements (left) and the dual solutions associated to J_1 (center) and J_2 (right).

In Fig. 11, we present the final mesh after 2 and 6 iterations of Algorithm 1 for the quantity of interest J_1. As in the previous example, the refinement occurs in some specific regions, such as those near Dirichlet-Neumann transitions and concavities on the boundary. Our results also show that the proposed method leads to the strong refinement near the interface between the necrotic core and the fibrosis, where stresses are localized because of the material heterogeneity. Conversely to the previous example, the refined meshes obtained for J_2 (not depicted) are very similar to those obtained for J_1.

Fig. 12 (left) depicts the relative goal-oriented error $|J_1(\mathbf{u}) - J_1(\mathbf{u}_h)|/|J_1(\mathbf{u})|$ versus the number N of cells in the mesh, both for uniform refinement (blue) and adaptive refinement (red). The stopping criterion ε has been fixed at 5.10^{-6}. Remark that, for the intial mesh $N = 1242$, the relative value of the discretization error is large (about 38 %), because the mesh does not resolve properly the discontinuity of material parameters E_n and E_s at the boundary of the necrotic core. The adaptive algorithm allows to recover this interface, as illustrated by Fig. 11, and to reduce the error, which is around 5 % after only two iterations. In Fig. 12 (right), we depict the effectivity indices for the global estimator η_h and the sum of local estimators $\Sigma_K \eta_K$. The same observations as in the previous example can be stated, and the estimators provide acceptable value of the *discretization error*. Moreover η_h performs better though it still underestimates slightly the error. Results we obtained for the quantity J_2 are very similar.
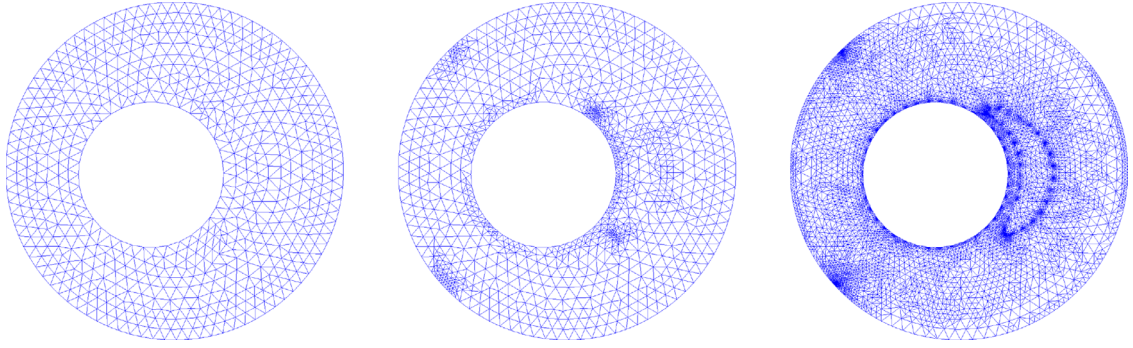
Fig. 11. Artery mesh. Refinement driven by the QoI J_1. Initial mesh (left) with 1242 cells and a relative error of 38.3 %, adapted meshes after 2 iterations (center) with 2079 cells and a relative error of 5.2 % and after 6 iterations (right) with 15028 cells and a relative error of 3.4 %.
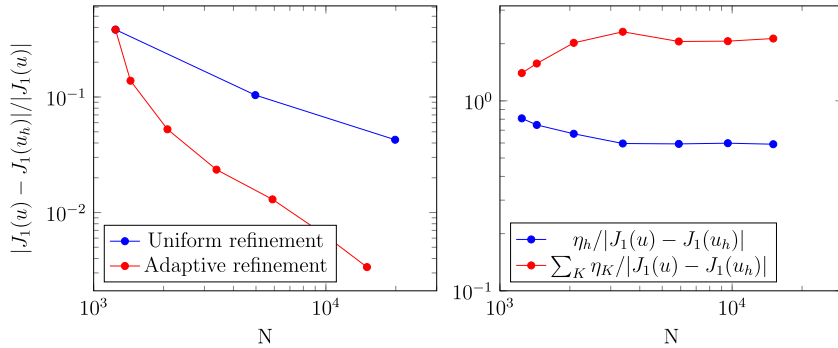

Fig. 12. Artery model. Left: relative error for the QoI J_1 *vs.* the number N of cells in the case of uniform (blue) and adaptive (red) refinement. Right: effectivity indices of η_h (blue) and $\Sigma_K \eta_K$ *vs.* the number of cells N for the QoI J_1. (For interpretation of the references to color in this figure legend, the reader is referred to the web version of this article.)

4. Discussion

In the first part, we discuss about the ability of the proposed methodology to assess and reduce the *discretization error*. In the second part, we comment on some further issues to improve and guarantee the accuracy of the error estimator, and to optimize the mesh refinement algorithm. Finally we address the issue of tackling more complex problems that arise in current practice for clinical biomechanics, and point out the main limitations of the current study as well as some perspectives.

4.1. Towards quantification of the discretization error: first achievements

The numerical results obtained in the last section show the ability of the proposed framework to provide relevant information about the *discretization error*: though the global estimator η_h provides only an approximation of the error in the quantity of interest $|J(\mathbf{u}) - J(\mathbf{u}_h)|$, this is often sufficient in practice. Moreover, the local estimators η_K provide a means to evaluate "relative" errors and thereby drive mesh refinement (Algorithm 1). Both the local and global errors can be significantly reduced without much computational effort. For instance, in the second test-case Section 3.2, and for J_1, the error is reduced by a factor of almost 4, after two successive refinements, and with only 20 % of extra cells. Similarly, for the third test-case Section 3.3, the error drops from 38.3 % to 5.3 %, approximately, after two successive refinements, with approximately 60 % of extra cells. In order to quantify more precisely the computational gains provided by the adaptive procedure, the computational time required to compute the error estimator and to regenerate or adapt the mesh should be thoroughly computed and analyzed, as was done for three-dimensional fracture problems treated by enriched finite element methods [31].

Let us emphasize the well-known fact that sources of *discretization errors* are *local*, and concentrated mostly in regions where the solution is not smooth, *e.g.,* subjected to strong variations, discontinuities or singularities. As a consequence, uniform refinement is highly suboptimal, while adaptive refinement performs much better by optimizing the number of elements, their size and location within the domain. Moreover, the proposed adaptive procedure is fully automatic, and no *a priori* knowledge of the critical regions is needed. For goal-oriented error estimation, the refined mesh obtained by the

algorithm can in fact be counter-intuitive, because it is driven by the sensitivity of the quantity of interest with respect to the local error. This sensitivity is obtained by solving the dual problem (see for instance Fig. 4 in Section 3.2) whose solution is, indeed, often not intuitive and difficult to interpret from a physical viewpoint.

In comparison to widespread error techniques implemented in most of commercial finite element software, the DWR technique allows to estimate and to improve the error for an arbitrary quantity of interest J. Each practitioner can choose the relevant quantity of interest J and obtain an approximation of the error on this quantity of interest $|J(\mathbf{u}) - J(\mathbf{u}_h)|$, as well as a map of the local error. The authors emphasize that the results obtained in the current study also demonstrate that the optimal refinement strategy depends significantly on the choice of the quantity of interest J. In general, such a goal-oriented refinement strategy leads to meshes which may differ significantly from those obtained by minimizing the error in energy. Remark that such goal-oriented approaches were also developed for the Zienkiewicz-Zhu error estimators [32] in [33,34] and for explicit residual based estimates in [35,36].

4.2. Some further mathematical and computational issues

It is desired that the global estimator η_h compute reliable information on the error in the quantity of interest $|J(\mathbf{u}) - J(\mathbf{u}_h)|$, providing quality measures to the user. In theory, this error is a *guaranteed upper bound*, with an explicit constant equal to 1. Yet, the theory assumes that the dual solution z is exactly known. This is never the case in practice as the dual problem is also solved using finite elements. Our numerical experiments show, however, that $|J(\mathbf{u}) - J(\mathbf{u}_h)|$ is estimated with reasonable accuracy and that the effectivity indices are close to 1, meaning that the approximate error on the quantity of interest is close to the (unknown) exact error on this quantity.

The numerical experiments provided in this paper confirm those of the literature on DWR technique, *e.g.,* [18,20,37] showing that the DWR is, in most situations, a reliable approach to compute goal-oriented error estimates. However, in certain situations, the DWR estimator is not as reliable as desired, since the effect of approximating the dual solution is difficult to control. This issue has been already pointed in the literature: see *e.g.,* [24,38,39] and earlier considerations in, *e.g.,* [37,40]. Especially, in [24] a simple situation where η_h provides a poor estimation on a coarse mesh is detailed. There is up to now no simple, cheap and general technique to address this issue, but first solutions have been suggested in [24,38,39]. They consist in modifying the DWR estimator so as to take into account the approximation of z. Also alternative new techniques have been derived recently to improve the robustness and accuracy of the DWR estimator, especially in the non-linear setting, see [41]. These are stimulating perspectives for further research. Moreover, the issue of computing a cheaper approximation of z, without compromising the reliability and efficiency of the estimator still needs to be addressed in depth.

Concerning mesh refinement, though the local estimator η_K combined with Algorithm 1 provides acceptable results, no effort has been spent on finding the value of parameter α in the Dörfler marking that yields improved refined meshes. On this topic, our global strategy for error estimation and mesh refinement is only a first attempt, and can be improved. For instance, in [25], an adaptive method based on specific weighting of the residuals of the primal and dual problems has been designed, and leads to quasi-optimal adapted meshes. Such a method could be tested and compared to the current one.

4.3. Applicability for patient-specific biomechanics?

Though the preliminary results presented in this paper demonstrate the relevance and practicability of *a posteriori* error estimators for providing quality control in quantities of interest to the biomechanics practitioner, and to drive mesh adaptation, much effort is still needed for the approaches developed here to address practical, personalized, clinically-relevant Finite Element simulations for biomechanical applications.

First, the compressible linear framework considered here is inadequate in practice and must be replaced by a fully non-linear, incompressible hyperelastic model, or even, in some situations, a, time and history dependent model [22]. Non-linearities also occur due to boundary conditions, when, for instance, contact or friction are present [7]. Moreover, most of the widespread quantities of interest in biomechanics are non-linear (norm of the displacements, local shear stress, maximum admissible stress and strain, etc). It is important to point out here that the DWR method for goal-oriented error estimation is already capable of tackling non-linearities: see, *e.g.,* [18] for the general framework, and, *e.g.,* [42,43] for first applications in non-linear elasticity and [35] for fracture mechanics. Ongoing work is about the adaptation of this non-linear framework to soft tissue models including incompressible hyperelasticity with active stress for muscle activation.

The major limitation of our work is that it assumes the mathematical model used to describe the image-based biomechanical problem to be able to reproduce accurately enough the physical reality. Unfortunately, in general, selecting the proper mathematical model for a given biomechanics problem is probably the most challenging part of the simulation process. The large, and increasing, number of papers dealing with the choice of constitutive model, for example, testifies for this difficulty. Indeed, there is still much to do to understand some complex physical and biological properties of human soft tissue, and to take them into account properly into current mathematical models. Another source of errors come from image reconstruction and in modelling appropriately boundary conditions. As a result, for a wide range of problems, modelling errors are the most significant. *A posteriori* error estimation may still be relevant for this purpose, since some works already deal with the error in the approximation of boundary conditions (see, *e.g.,* [44]) or more generally modelling errors

(see, *e.g.*, [45,46], which both rely also on dual weighted residuals). Yet, estimating rigorously and systematically the impact of these errors is extremely challenging, in particular when dealing with patient-specific simulations. Dealing with this issue is the focus of ongoing research in our teams but is far beyond the scope of this paper. Particularly, future research will be focused on scenarios where validation is possible using phantom or *in vivo* measurements. We made a first attempt in this direction in Section 3.1, which is encouraging, but limited because of the linear setting assumed in this paper, and because the test-case is not patient-specific. Note however that for patient-specific, *in vivo*, data, validation remains difficult, since one needs to recover accurately the material parameters of the soft tissue, and to take into account uncertainties in the measurements.

Additionally, We would like to make the following remarks. The first problem which must be addressed is the choice of a model (hyperelastic, viscous, porous, single/multi-scale...). The chosen model has parameters which must be estimated through inverse analysis. Once estimates, or probability distributions for these parameters are available, their importance on quantities of interest must be evaluated, through sensitivity analysis and uncertainty quantification. The major difficulty is, therefore, to select the proper model, and its parameters for a given patient. As *in vivo* experiments are in general not possible, data must be extracted as the patient is being treated, *e.g.*, during an operation. This can be done using Bayesian methods, which provide a reconciliation between expert knowledge on patient cohorts (prior) and actual properties of a given patient [47,48]. Real-time machine-learning-like methods such as Kalman filters demonstrated as well promising results [49,50]. To evaluate the effects of uncertainties on such material parameters, accelerated Monte-Carlo methods are possible avenues of investigation [51]. An exciting question is the comparative usefulness and combination of physical models (potentially learnt during medical treatment) and machine-learning algorithms, mostly based on data acquired during the intervention. Last but not least, note that the DWR method is based on optimal control principles, that makes it suitable for extensions to parameter calibration (viewed as an optimal control problem). In such a setting, it allows to combine sensitivity analysis with goal-oriented *a posteriori* error estimation, see [52]. In the same spirit, the interplay between *a posteriori* error estimation and uncertainty quantification has been object of recent research interests [53,54].

We also note that if users can obtain some estimate, even rough, of modelling errors, they will also be able to compare discretization and model errors. This enables the coarsening of the mesh if the discretization error is unnecessarily small in comparison to the modelling error as is done, *e.g.*, in [55] for adaptive scale selection. Conversely, for specific applications where modelling errors are small or moderate, the mesh can be refined efficiently to increase the precision, especially when discretization errors are far away from being negligible (see Section 3.3).

With our methodology, practitioners spending a large amount of time and effort in patient-specific mesh generation can obtain useful information on the impact of the quality of the mesh on quantities of interest to them. This information goes well beyond purely geometrical criteria for the regularity of the elements which are typically provided in commercial software.

This information can be used directly to optimize the choice of the discretization/mesh in view of minimizing the error on a specific quantity of interest. Fast/real-time numerical methods which provide real-time predictions have been intensively researched since the beginning of the 1990's. Those approaches are critical to build surgical planning and guidance tools, for example. Reliable error estimation is critical in these situations to guarantee the accuracy, but has been extremely scarcely addressed in the literature. As a first step in this direction, the recent work of [16] provides a real-time mesh refinement algorithm for needle insertion. Mesh refinement is driven by a ZZ error estimate, for the global norm. It would be interesting to extend such a method for goal-oriented error estimation, *e.g.*, on the motion of a target, or reaction/friction force along the needle shaft.

We should also mention alternative approaches to (implicit, standard) finite elements for fast nonlinear finite element analysis: for instance the solution of total lagrangian formulation of the equilibrium equations on graphics processing unit for neurosurgical simulation [56], or model order reduction techniques for the real-time, interactive simulation of tissue tearing during laparoscopic surgery [57].

A perspective consists in extending the current framework to such numerical methods where error control is particularly demanding. For explicit approaches, the interplay between the choice of the time-step and that of the mesh size is a difficult topic, especially for domains with significant stiffness differences where adaptive and multi-time-step schemes should be investigated.

5. Conclusions

We devised a framework to estimate and to reduce the discretization error in finite element simulation, that arises from patient-specific meshing in computer-assisted surgery. The main tools of this framework are the Dual Weighted Residual method for *a posteriori* error estimation associated to a user-defined quantity of interest, and a mesh-refinement algorithm. We considered a validation using experiments in silicone samples, and two scenarios, inspired from a tongue and an artery geometry, and with a simplified setting (plane linearized elasticity). The results are encouraging and demonstrate the feasibility of our methodology. Main perspectives are the extension of the proposed framework to more complex three-dimensional models including geometric and material non-linearities, as well as the estimation of modelling errors. Moreover, an important issue concerns thorough validation of the methodology using experimental measurements made on phantom or *in vivo*.

Acknowledgments

References

[1] T.E. Yankeelov, N. Atuegwu, D. Hormuth, J.A. Weis, S.L. Barnes, M.I. Miga, E.C. Rericha, V. Quaranta, Clinically relevant modeling of tumor growth and treatment response, Sci. Translat. Med. 5 (187) (2013). 187ps9–187ps9

[2] A. Romo, P. Badel, A. Duprey, J.-P. Favre, S. Avril, In vitro analysis of localized aneurysm rupture, J. Biomech. 47 (3) (2014) 607–616.

[3] H. Schmidt, F. Galbusera, A. Rohlmann, T. Zander, H.-J. Wilke, Effect of multilevel lumbar disc arthroplasty on spine kinematics and facet joint loads in flexion and extension: a finite element analysis, Eur. Spine J. 21 (5) (2012) 663–674.

[4] D. Perrin, P. Badel, L. Orgéas, C. Geindreau, A. Dumenil, J.-N. Albertini, S. Avril, Patient-specific numerical simulation of stent-graft deployment: validation on three clinical cases, J. Biomech. 48 (10) (2015) 1868–1875.

[5] V. Luboz, M. Bailet, C. Boichon Grivot, M. Rochette, B. Diot, M. Bucki, Y. Payan, Personalized modeling for real-time pressure ulcer prevention in sitting posture, J. Tissue Viab. 27 (1) (2018) 54–58.

[6] S. Buchaillard, M. Brix, P. Perrier, Y. Payan, Simulations of the consequences of tongue surgery on tongue mobility: implications for speech production in post-surgery conditions, Int. J. Med. Robot. Comput. Ass. Surg. 3 (3) (2007) 252–261.

[7] H. Courtecuisse, J. Allard, P. Kerfriden, S.P.A. Bordas, S. Cotin, C. Duriez, Real-time simulation of contact and cutting of heterogeneous soft-tissues, Med. Image Anal. 18 (2) (2014) 394–410.

[8] T. Grätsch, K.-J. Bathe, A posteriori error estimation techniques in practical finite element analysis, Comput. Struct. 83 (4) (2005) 235–265.

[9] A. Bijar, P.-Y. Rohan, P. Perrier, Y. Payan, Atlas-based automatic generation of subject-specific finite element tongue meshes, Ann. Biomed. Eng. 44 (1) (2016) 16–34.

[10] F. Shang, Y. Gan, Y. Guo, Hexahedral mesh generation via constrained quadrilateralization, PLoS ONE 12 (5) (2017).

[11] J. Shepherd, C. Johnson, Hexahedral mesh generation for biomedical models in SCIRun, Eng. Comput. 25 (2009) 97–114.

[12] M. Bucki, C. Lobos, Y. Payan, N. Hitschfeld, Jacobian-based repair method for finite element meshes after registration, Eng. Comput. 27 (3) (2011) 285–297.

[13] M. Ainsworth, J.T. Oden, A posteriori error estimation in finite element analysis, Pure and Applied Mathematics, Wiley-Interscience, New York, 2000.

[14] R. Verfürth, A posteriori error estimation techniques for finite element methods, Numerical Mathematics and Scientific Computation, Oxford University Press, Oxford, 2013.

[15] R.H. Nochetto, K.G. Siebert, A. Veeser, Theory of adaptive finite element methods: an introduction, in: Multiscale, Nonlinear and Adaptive Approximation, Springer, Berlin, 2009, pp. 409–542.

[16] H.P. Bui, S. Tomar, H. Courtecuisse, S. Cotin, S.P.A. Bordas, Real-time error control for surgical simulation, IEEE Trans. Biomed. Eng. 65 (3) (2018) 596–607.

[17] R. Becker, R. Rannacher, A feed-back approach to error control in finite element methods: basic analysis and examples, East-West J. Numer. Math. 4 (4) (1996) 237–264.

[18] R. Becker, R. Rannacher, An optimal control approach to a posteriori error estimation in finite element methods, Acta Numer. 10 (2001) 1–102.

[19] , Automated Solution of Differential Equations by The finite Element Method. The FEniCS book, in: A. Logg, K.-A. Mardal, G.N. Wells (Eds.), Lecture Notes in Computational Science and Engineering, 84, Springer, Heidelberg, 2012.

[20] M.E. Rognes, A. Logg, Automated goal-oriented error control I: Stationary variational problems, SIAM J. Sci. Comput. 35 (3) (2013) C173–C193.

[21] S.C. Cowin, J.D. Humphrey, Cardiovascular Soft Tissue Mechanics, Springer, 2001.

[22] Y. Payan, J. Ohayon, Biomechanics of living organs: hyperelastic constitutive laws for finite element modeling, Academic Press Series in Biomedical Engineering, Elsevier, 2017.

[23] A. Ern, J.-L. Guermond, Theory and Practice of Finite Elements, Applied Mathematical Sciences, 159, Springer-Verlag, New York, 2004.

[24] R.H. Nochetto, A. Veeser, M. Verani, A safeguarded dual weighted residual method, IMA J. Numer. Anal. 29 (1) (2009) 126–140.

[25] R. Becker, E. Estecahandy, D. Trujillo, Weighted marking for goal-oriented adaptive finite element methods, SIAM J. Numer. Anal. 49 (6) (2011) 2451–2469.

[26] W. Dörfler, A convergent adaptive algorithm for Poisson's equation, SIAM J. Numer. Anal. 33 (3) (1996) 1106–1124.

[27] S. Le Floc'h, J. Ohayon, P. Tracqui, G. Finet, A.M. Gharib, R.L. Maurice, G. Cloutier, R.I. Pettigrew, Vulnerable atherosclerotic plaque elasticity reconstruction based on a segmentation-driven optimization procedure using strain measurements: theoretical framework, IEEE Trans. Med. Imaging 28 (7) (2009) 1126–1137.

[28] L. Meunier, G. Chagnon, D. Favier, L. Orgéas, P. Vacher, Mechanical experimental characterisation and numerical modelling of an unfilled silicone rubber, Polymer Test. 27 (6) (2008) 765–777.

[29] J.M. Gerard, J. Ohayon, V. Luboz, P. Perrier, Y. Payan, Non-linear elastic properties of the lingual and facial tissues assessed by indentation technique: Application to the biomechanics of speech production, Med. Eng. Phys. 27 (10) (2005) 884–892.

[30] P. Tracqui, J. Ohayon, Transmission of mechanical stresses within the cytoskeleton of adherent cells: a theoretical analysis based on a multi-component cell model, Acta Biotheor. 52 (4) (2004) 323–341.

[31] Y. Jin, O. González-Estrada, O. Pierard, S.P.A. Bordas, Error-controlled adaptive extended finite element method for 3D linear elastic crack propagation, Comput. Methods Appl. Mech. Eng. 318 (2017) 319–348.

[32] O.C. Zienkiewicz, J.Z. Zhu, A simple error estimator and adaptive procedure for practical engineering analysis, Int. J. Numer. Methods Eng. 24 (2) (1987) 337–357.

[33] O.A. González-Estrada, E. Nadal, J. Ródenas, P. Kerfriden, S.P.A. Bordas, F. Fuenmayor, Mesh adaptivity driven by goal-oriented locally equilibrated superconvergent patch recovery, Comput. Mech. 53 (5) (2014) 957–976.

[34] O.A. González-Estrada, J.J. Ródenas, S.P.A. Bordas, E. Nadal, P. Kerfriden, F.J. Fuenmayor, Locally equilibrated stress recovery for goal oriented error estimation in the extended finite element method, Comput. Struct. 152 (2015) 1–10.

[35] M. Rüter, T. Gerasimov, E. Stein, Goal-oriented explicit residual-type error estimates in XFEM, Comput. Mech. 52 (2) (2013) 361–376.

[36] T. Wick, Goal functional evaluations for phase-field fracture using PU-based DWR mesh adaptivity, Comput. Mech. 57 (6) (2016) 1017–1035.

[37] M.B. Giles, E. Süli, Adjoint methods for PDEs: a posteriori error analysis and postprocessing by duality, Acta Numer. 11 (2002) 145–236.

[38] M. Ainsworth, R. Rankin, Guaranteed computable bounds on quantities of interest in finite element computations, Int. J. Numer. Methods Eng. 89 (13) (2012) 1605–1634.

[39] C. Carstensen, Estimation of higher Sobolev norm from lower order approximation, SIAM J. Numer. Anal. 42 (5) (2005) 2136–2147.
[40] W. Bangerth, R. Rannacher, Adaptive finite element methods for differential equations, Lectures in Mathematics ETH Zürich, Birkhäuser Verlag, Basel, 2003.
[41] B. Endtmayer, U. Langer, T. Wick, Two-side a posteriori error estimates for the DWR method, arXiv:1811.07586 (2018).
[42] F. Larsson, P. Hansbo, K. Runesson, Strategies for computing goal-oriented a posteriori error measures in non-linear elasticity, Int. J. Numer. Methods Eng. 55 (8) (2002) 879–894.
[43] J.P. Whiteley, S.J. Tavener, Error estimation and adaptivity for incompressible hyperelasticity, Int. J. Numer. Methods Eng. 99 (5) (2014) 313–332.
[44] S. Repin, S. Sauter, A. Smolianski, A posteriori error estimation for the Dirichlet problem with account of the error in the approximation of boundary conditions, Computing 70 (3) (2003) 205–233.
[45] J.T. Oden, S. Prudhomme, Estimation of modeling error in computational mechanics, J. Comput. Phys. 182 (2) (2002) 496–515.
[46] M. Braack, A. Ern, A posteriori control of modeling errors and discretization errors, SIAM J. Multiscale Model. Simul. 1 (2) (2003) 221–238.
[47] H. Rappel, L.A. Beex, J.S. Hale, L. Noels, S.P.A. Bordas, A tutorial on bayesian inference to identify material parameters in solid mechanics, Arch. Comput. Methods Eng. (2019). (to appear).
[48] H. Rappel, L.A. Beex, S.P.A. Bordas, Bayesian inference to identify parameters in viscoelasticity, Mech. Time Depend. Mater. 22 (2) (2018) 251–258.
[49] P. Moireau, D. Chapelle, P. Le Tallec, Filtering for distributed mechanical systems using position measurements: perspectives in medical imaging, Inverse Probl. 25 (3) (2009) 035010, 25.
[50] N. Haouchine, J. Dequidt, I. Peterlik, E. Kerrien, M.-O. Berger, S. Cotin, Image-guided simulation of heterogeneous tissue deformation for augmented reality during hepatic surgery, in: Proceedings of the IEEE International Symposium on Mixed and Augmented Reality (ISMAR), IEEE, 2013, pp. 199–208.
[51] P. Hauseux, J.S. Hale, S.P.A. Bordas, Accelerating Monte Carlo estimation with derivatives of high-level finite element models, Comput. Methods Appl. Mech. Eng. 318 (2017) 917–936.
[52] R. Becker, B. Vexler, Mesh refinement and numerical sensitivity analysis for parameter calibration of partial differential equations, J. Comput. Phys. 206 (1) (2005) 95–110.
[53] M. Eigel, C. Merdon, J. Neumann, An adaptive multilevel Monte Carlo method with stochastic bounds for quantities of interest with uncertain data, SIAM/ASA J. Uncerta. Quant. 4 (1) (2016) 1219–1245.
[54] D. Guignard, F. Nobile, M. Picasso, A posteriori error estimation for elliptic partial differential equations with small uncertainties, Numer. Methods Partial Differ. Equ. 32 (1) (2016) 175–212.
[55] A. Akbari Rahimabadi, P. Kerfriden, S.P.A. Bordas, Scale selection in nonlinear fracture mechanics of heterogeneous materials, Philosoph. Mag. 95 (28–30) (2015) 3328–3347.
[56] G.R. Joldes, A. Wittek, K. Miller, Suite of finite element algorithms for accurate computation of soft tissue deformation for surgical simulation, Med. Image Anal. 13 (6) (2009) 912–919.
[57] S. Niroomandi, I. Alfaro, D. Gonzalez, E. Cueto, F. Chinesta, Real-time simulation of surgery by reduced-order modeling and X-FEM techniques, Int. J. Numer. Methods Biomed. Eng. 28 (5) (2012) 574–588.